New Forcefields for Modeling Biomineralization Processes

Colin L. Freeman* and John H. Harding

Department of Engineering Materials, University of Sheffield, Sir Robert Hadfield Building, Mappin Street, Sheffield S1 3JD, U.K.

David J. Cooke and James A. Elliott

Department of Materials Science and Metallurgy, University of Cambridge, New Museums Site, Pembroke Street, Cambridge CB2 3QZ, U.K.

Jennifer S. Lardge and Dorothy M. Duffy

Department of Physics and Astronomy, University College London, Gower Street, London WC1E 6BT, U.K.

Received: March 8, 2007; In Final Form: June 5, 2007

A generic method for producing potentials to model organic−mineral systems is proposed. The method uses existing potentials for the components of the system and produces cross-term potentials between these components. The existing potentials are fitted to known mineral structures modeled with charges that mimic the Coulombic potential at the organic−mineral interface. The method has been applied to supply a set of potentials to model calcite biomineralization, including water−calcite, bicarbonate ions, and a set of organic functional groups with calcite. Tests comparing the results from ab initio and other potential-based calculations demonstrate that the new potential set is reliable and accurate.

1. Introduction

Theoretical models are increasingly being applied to processes involving organic−mineral interfaces such as biomineralization with some success (for a summary, see ref 1). However, drawbacks remain with all theoretical approaches. Ab initio methods cannot generally be taken beyond a few hundred atoms, making the scale of biomineralization processes difficult to model. The use of mesoscale methods can give very useful data but blurs direct atom−atom interactions, which may contain some of the important chemistry. Therefore, potential-based methods provide a vital component for modeling biomineralization. The difficulty with using classical methods is the need for a reliable and robust potential set. Any successful model must simulate the mineral, the organic molecules, the solvent (usually water), and the interactions between these three groups (cross-term potentials). Biomineralization by its very nature bridges two theoretical fields, one modeling inorganic minerals and the other modeling organic molecules in solvent environments. Both fields have reliable potential models that have been applied across a wide range of problems but combining them to model biominerals presents challenges.

An obvious method for combining the two sets to generate cross-term potentials would be to use the Lorentz−Berthelot mixing rules. Previous studies[2,3] have demonstrated that these severely over-estimate binding energies at the interface. This problem stems from the different theoretical approach of the two potential sets. Mineral potentials are generally based on the Born model of solids, where the interactions between atoms are represented as long-range electrostatics and short-range forces that cover both the van der Waals attraction and Pauli repulsion. These models rely on a largely ionic description where the interatomic interactions are dominated by the Coulombic terms. On the other hand, organic potentials often use relatively small charges on the atoms together with strong bond terms. Therefore, a combination of the two models is prone to difficulty, as the atomic charges, particularly on atoms shared between the systems (such as oxygen), are not consistent. This issue could be resolved by a systematic refitting of both potential sets, but this would involve large computational expense and would show disregard for the reliability of the potentials currently available. Since both achieve a good level of accuracy within their respective systems, it would be wasteful to begin again; in addition, there is the question of whether we should use an "ionic" or "covalent" model?

An alternative is to recast the interatomic cross-term potentials to fit the different charges between the systems. This method was used by Schröder et al.[4] to look at zeolites with methanoic acid but can be equally applied to biominerals, as has been demonstrated by de Leeuw et al.[5] and Duffy and Harding[2] with success. So far, potentials have only been fitted to a limited number of organic molecules and functional groups. This needs to be expanded to allow us to study a range of different biomineralization processes. In addition, the fitting procedure varies between systems, so no standard method exists for producing the cross-term potentials.

A related issue to the development of organic/mineral potential parameters is the need for a reliable model for water, both with the organic system and at the mineral surface. Additionally, as it has been shown that water dissociates on many mineral surfaces, we must also be able to consider hydroxide groups on the mineral surface. Ideally, this would be achieved via an ionizable model, but this presents serious problems. Two models do exist in the literature: Halley and co workers[6] have developed a potential based on the Stillinger−David model,[7,8] and Litton and Garofalini[9] have used a damped

* Address correspondence to this author. Phone: +44 (0)114 222 6021. Fax: +44 (0)114 222 5943. E-mail: c.l.freeman@sheffield.ac.uk.

10.1021/jp071887p CCC: $37.00
Published on Web 07/24/2007 PAGE EST: 9

electrostatic model. Both have been applied successfully to studying the mineral/water interface. However, neither of these models (or even this class of model) have been used in simulating organic systems. Organic systems have been adapted to use simple models, often of the TIP*n*P variety (where *n* equals three or four). To use the former more complex water models would entail re-examining the entire database of organic molecular interactions, a formidable task.

The alternative to using an ionizable model for water is to develop separate, yet compatible, models for molecular water and hydroxide groups. This is an approach followed in the CLAYFF model[10] and in developing a model to study the rutile (110)/water interface,[11] where both used the SPC/E[12] model for molecular water. Parker and co-workers, in modeling hydroxylated and hydrated surfaces of a range of inorganic minerals, have also employed such methodologies extensively.[13,14] This has included modeling the hydroxylation and hydration of calcite surfaces,[15] although their model did not include the bicarbonate ion.

Earlier studies have developed potentials that have proved effective in analyzing particular problems, but we would argue that a generic set of potentials is needed to cover the range of possible cross-terms that occur in biomineral systems. In addition, previous methods have utilized particular mineral and organic forcefields, restricting future users. In this paper, we describe and test a methodology that can be used to produce a robust and reliable potential set for the majority of mineral/organic/water forcefields and most biomineral systems without the need for systematic fitting in each case.

2. Potential Development

The principles of our potential development are twofold: First, we wish to use existing potentials wherever possible to model the components of the system and only generate new potentials to model the interactions between these components; second, the cross-term potentials should be derived, as much as is possible, via a standard methodology that does not require expensive fitting proceedures. Below is a brief summary of our approach to achieving these objectives:

(1) We have used the method described by Schröder et al.[4] which refits existing potentials to mineral structures so that they are consistent with the Coulombic interactions between the mineral and nonmineral atoms. (2) When the refitting described above is not possible, then further potentials have been generated by fitting to mineral structures. (3) Potentials that do not cover strong Coulombic interactions (and are therefore not appropriate for the Schrörder method) are chosen on the basis of their presence within the organic or mineral forcefield and are generated by following modified mixing rules. (4) If no mixing rules can be used due to the lack of the necessary mineral−mineral potential, the mineral−organic potential used is a duplicate of the appropriate organic potential.

There are many different biomineralization processes and biominerals. For the purposes of describing our methodology for generating cross-term potentials, it is easiest to demonstrate with a reference to a particular biomineral: we choose calcite, $CaCO_3$, as it is one of the most common biomaterials. Throughout this work we have used the potential model developed by Pavese et al.[16,17] for calcite, which has been demonstrated to successfully reproduce the properties of calcite and other carbonate materials (e.g., see ref 18). To increase computational efficiency, and because they are not included in the organic potential libraries, we have removed the polarization shell from the carbonate oxygen. Therefore, our oxygen atoms all carry a charge of $-1.045e$ as described in ref 16. In addition, we have described the O−O potential in terms of a Born−Mayer potential. The *AMBER*[19] forcefield parameters were used to model the organic molecules present. The water model used was TIP3P,[20] which is fully consistent with the *AMBER* (and *CHARMM*) forcefield removing any requirements to re-fit the water−organic interactions. Although the following work uses particular forcefields, the methods described for the potential development are generic and, in principle, could be used with other organic/water/mineral potentials.

In the following sections, we discuss the methodology used to generate a series of potentials for mineral−organic molecule and mineral−water interactions.

2.1. Organic−Mineral Interactions. A crucial problem for modeling the organic−mineral interface is the large charge disparity between the two systems. As alluded to in the Introduction, this is accounted for by applying the method described by Schröder et al.[4] Given a mineral atom, A, and an organic atom, B, there are two main conditions to the Schröder method

$$q_{\mathrm{Anew}} q_{\mathrm{Bnew}} = q_{\mathrm{Amineral}} q_{\mathrm{Borganic}} \tag{1}$$

and

$$\sum_I q_{I\mathrm{new}} = 0 \tag{2}$$

The principle of the method is to derive a new cross-term potential for the interatomic interaction between two atoms by fitting the potential to a new system (generally a mineral containing atoms A and B) in which the Coulombic interaction between the atoms is duplicated (eq 1). The values of q_{Anew} and q_{Bnew} along with any other atoms (I) within the system must satisfy eq 2; these charges can be determined by scaling the values of the atoms within the original mineral

$$q_I = \alpha_I q_{\mathrm{Bnew}} \tag{3}$$

where

$$\alpha_I = \frac{q_{I\mathrm{mineral}}}{q_{\mathrm{Bmineral}}} \tag{4}$$

This approach reduces eq 1 to

$$\alpha_{\mathrm{A}} q_{\mathrm{Bnew}}^2 = q_{\mathrm{Amineral}} q_{\mathrm{Borganic}} \tag{5}$$

which gives a value for q_{Bnew} from which all the other values of q_I can be determined.

The cross-term potential that is desired can now be fitted to this new system by forcing the repulsive term of the potential to decrease to maintain the crystal lattice (which would otherwise change due to the new charges). This provides a new interatomic potential that is consistent with the reduced Coulombic interactions present in the mineral−organic interactions.

2.1.1. Example−Calcite and Alcohol. To model the interactions between the calcite crystal and an alcohol molecule, there must be a cross-term potential for the Ca−O bond. The calcite mineral can be used to generate this cross-term potential, as it contains both Ca and O and an interatomic Buckingham potential between them. In the Pavese forcefield, we have Ca^{2+} and $O_{\mathrm{mineral}}{}^{1.045-}$; therefore, from eq 4, $\alpha_I = -1.91$. In the *AMBER* (organic) forcefield, $q_{\mathrm{Oorganic}} = -0.67e$ within the alcohol functional group. Substituting the charges and α_I into eq 5 provides $q_{\mathrm{Onew}} = -0.838$. With the use of the new oxygen charge, the calcium and carbon charges are reassigned using eq 3. These new charges are now used for modeling the calcite

crystal with the mineral (Pavese) forcefield. The *A* parameter of the Ca−O Buckingham potential interatomic potential is fitted to the calcite lattice parameters, reducing it to a value of 1000.0 eV. See Table 1 for all the Buckingham potentials fitted in this method ($Ca-O_{alcohol}$, $Ca-O_{ether}$, and $Ca-O_{acid}$).

2.1.2. Additional Cross-Terms. There are several possible nonbonded potentials that can be considered for the mineral−organic interactions. The interaction between the Ca^{2+} ion and oxygen atoms in the organic system is crucial, due to the strong Coulombic attraction between them. For other atoms, a potential may not be needed, since the Coulombic interaction is repulsive or very weak. Choosing the particular potentials to model can become arbitrary. We therefore define our choice of potential interactions by those present within the organic forcefield. If atom A of an A−B organic potential is also present in the mineral, then a potential exists between the mineral atom A and the organic atom B. For example, if there is a C−O nonbonded potential in the organic forcefield, we include $C_{mineral}-O_{organic}$ and $C_{organic}-O_{mineral}$ cross-term potentials in our model.

For this scenario, a modified set of mixing rules are used to produce the cross-term potential.

Organic potentials are generally of the Lennard−Jones (LJ) 12-6 form and are combined to give interatomic potentials by using the standard Lorentz−Berthelot mixing rules, i.e.

$$E_0 = \sqrt{E_0(1)E_0(2)} \tag{6}$$

and

$$R_0 = \frac{R_0(1) + R_0(2)}{2} \tag{7}$$

These rules cannot be implemented with the commonly used Buckingham potentials of mineral forcefields; therefore, the $O_{mineral}-O_{mineral}$ Buckingham potential has been fitted to a LJ 12-6 potential (see Table 1). This potential was then used with the mixing rules to generate additional cross-term potentials only (e.g., $O_{mineral}-O_{organic}$ but not to substitute for the $O_{mineral}-O_{mineral}$ interaction). When no appropriate inorganic potential exists for the fit (i.e., there is no C−C potential in the mineral potential), then we duplicate the organic potential for the mineral−organic potential. So, for the $C_{mineral}-O_{organic}$ potential, we have used the $C_{organic}-O_{organic}$ potential. By using LJ potentials, the cross-terms remain consistent with the organic forcefield, and we are able to utilize the straightforward mixing rules. These cross-term potentials cover the generally weak interactions between Coulombically repelled atoms and those with relatively weak attractions; therefore, it is not essential to derive the potentials from a charge viewpoint as with the Schröder method.

It should be noted that this method means that a new set of potentials should be generated whenever the organic forcefield is changed. For example, if the $O_{organic}-O_{organic}$ nonbonded potential has changed for a new molecule, then the cross-terms should also change according to the mixing rules described above. One could consider re-fitting the Coulombic interactions if the charges on the functional groups changed between molecules, but this should only be necessary if the charge was significantly different.

The methods described above use a systematic approach for generating the cross-term potentials between the organic and mineral components of the system. This method also ensures that the reliable forcefields for the two separate systems are still used internally, ensuring that accuracy is maintained for modeling the molecules and minerals.

TABLE 1: List of Cross-Term Potentials Derived in This Paper and Used for the Potential Tests Described in the Results Section

Buckingham potentials ($A\exp(-\rho/r) - C/r^6$)				
		A (eV)	ρ (Å)	C (eV Å^{-6})
Ca	$O_{alcohol}$	1000.0	0.297	0.0
Ca	O_{ether}	690.0	0.297	0.0
Ca	O_{acid} (OH)[a]	850.0	0.297	0.0
Ca	O_{acid} (C═O)[b]	675.0	0.297	0.0
Ca	O_{water}	1186.6	0.297	0.0
Ca	$O_{hydroxyl}$	2251.05	0.297	0.0
Ca	$O_{bicarbonate}$	1155.52	0.297	0.0
all O	all O[c]	16372.33	0.213	0.0
Lennard−Jones 12-6 potentials ($E_0[(R_0/r)^{12} - 2(R_0/r)^6]$)				
		E_0 (eV)	R_0 (Å)	
		calcite−alcohol		
O	O	0.00218	3.721	
O	H (C−H)	0.000595	3.387	
O	C	0.00157	3.908	
C	O	0.00658	3.629	
C	H (C−H)	0.00180	3.295	
C	C	0.00475	3.816	
		calcite−ether		
O	O	0.000595	3.387	
O	H	0.000595	3.387	
O	C	0.00157	3.908	
C	O	0.00180	3.295	
C	H	0.00180	3.295	
C	C	0.00475	3.816	
		calcite−acid		
O	O (OH)[a]	0.00218	3.721	
O	O (C═O)[b]	0.00218	3.661	
O	H (C−H)	0.000582	3.459	
O	C	0.00139	3.908	
C	O (OH)[a]	0.00584	3.629	
C	O (C═O)[b]	0.00583	3.569	
C	H (C−H)	0.00156	3.367	
C	C	0.00373	3.816	
		calcite−calcite[d]		
O	O	0.000520	4.0	
Lennard−Jones 9-6 potentials ($E_0[2(R_0/r)^9 - 3(R_0/r)^6]$)				
		E_0 (eV)	R_0 (Å)	
$O_{calcite}$	O_{water}	0.00130	4.63	
$O_{carbonate}$	H_{ion}	0.00730	2.71	
$O_{hydroxyl}$	H_{ion}	0.00730	2.71	
$O_{bicarbonate}$	H_{ion}	0.00730	2.71	
intramolecular Morse potentials[e] ($D(1 - \exp(-\beta(r - r_0))) - D$				
		D (eV)	β (Å^{-1})	r_0 (Å)
$O_{hydroxyl}$	H	7.053	3.175	0.9429
$O_{bicarbonate}$	H	7.053	3.175	0.9429

[a] (OH) refers to the alcohol oxygen (i.e., with an O−H bond). [b] (C═O) refers to the aldehyde oxygen (i.e., the oxygen double bonded to the carbon). [c] The Buckingham potential used for all the calcite O−O (and their ions) interactions, as taken from the Pavese potential set. [d] This is the LJ 12-6 potential fitted to the Buckingham O−O potential for use exclusively for mixing with the other organic potentials. [e] Potential of Baram and Parker;[25] Coulombic interactions are subtracted from these bonded interactions.

2.2. Water−Mineral Interactions. The potential sets designed for water interactions are generally compatible with organic forcefields but not mineral ones. Again, the method of Schröder et al. described in the previous section was used to scale the interatomic ($Ca-O_{water}$) potential using calcite as a reference mineral. The remaining potentials required for the

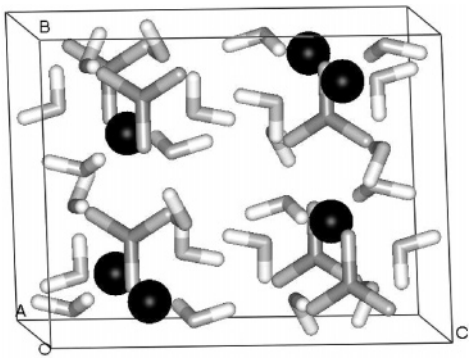

Figure 1. Ikaite,[21] a calcium carbonate hexahydrate, $CaCO_3 \cdot (H_2O)_6$. Key: calcium, black; carbon, dark gray; oxygen, light gray; hydrogen, white.

TABLE 2: Crystallographic Data (1) Comparing Experimental and Calculated Data for Ikaite and (2) for Our Presumed Structure of Calcium Bicarbonate Using DFT and the Potential Models Derived in This Work

	ikaite		calcium bicarbonate	
	experimental	TIP3P	DFT	potential
space group	*C*12/*c*1	*C*2/*c*	*P*1	*P*1
a (Å)	8.87	9.23	7.96	8.15
b (Å)	8.23	8.18	7.61	7.00
c (Å)	11.02	10.5	9.1	9.31
α (deg)	90.0	90.0	90.0	90.0
β (deg)	110.2	108.8	90.0	90.0
γ (deg)	90.0	90.0	81.8	80.3

calcite−water system are fitted to the structure of ikaite,[21] a calcium carbonate hexahydrate, $CaCO_3 \cdot (H_2O)_6$ (see Figure 1). This method was successfully used by de Leeuw and Parker[22] for generating a calcite−water potential set (using an oxygen shell for both calcite and water, which our model does not include). The interatomic interactions present between mineral and water molecule are designed to be consistent with those of the water forcefield. The TIP3P water forcefield defines the intermolecular interactions through the oxygen only (i.e., there are no H−X potentials, where X is an atom not within the water molecule). Therefore, only an oxygen−mineral potential is considered. We fitted a LJ 9-6 potential to the O−O interactions (as this was found to best fit the crystallographic data) using the General Utility Lattice Program (GULP).[23,24] The potentials are shown in Table 1, and the calculated crystallographic results are shown in Table 2.

2.3. Dissociated Water−Mineral Interactions. We have developed separate potential parameters to model dissociated water interacting in the form of hydroxyl and bicarbonate with calcite surfaces that are compatible with the other potential sets described earlier, using the same scheme described above for fitting the calcite−organic potential parameters. The O−H bond in the hydroxide group and the bicarbonate is described using the Morse potential of Baram and Parker.[25] The additional parameters that were required were those of the Ca^{2+} ion interacting with the hydroxide group and the intermolecular interactions between hydrogen and oxygen. These were obtained from the mineral portlandite (calcium hydroxide as shown in Figure 2) and a theoretically calculated structure for solid calcium bicarbonate.

2.3.1. Calcium−Hydroxide Interactions. Our starting point for this study was the experimentally determined structure of Desgranges et al.,[26] which has lattice parameters of $a = b =$ 3.59 Å, $c = 4.91$ Å, $\alpha = \beta = 90°$, and $\gamma = 120°$. In addition, experimentally determined values for the elastic constants (excluding C_{14}) are also available[27] and were used to verify the quality of the potential parameters fitted. Additional reference was also made to ab initio calculations by relaxing the experimentally determined crystal structure with density functional theory (DFT) as implemented in the *CASTEP3* code[28] using the generalized gradient approximation (GGA) basis sets with a cutoff of 500 eV and 5 5 5 *k*-point grid. This gave a structure with relaxed parameters $a = b = 3.57$ Å, $c = 4.88$ Å, $\alpha = \beta = 90°$, and $\gamma = 120°$.

TABLE 3: Structural Parameters Calculated for Portlandite Using the Potential Set Developed in This Paper, Other Potentials Specifically Fitted to Portlandite, and Experimental Values

			elastic constants (GPa)					
	a (Å)	*c* (Å)	C_{11}	C_{12}	C_{13}	C_{33}	C_{44}	C_{66}
experiment	3.59	4.91	99.3	36.2	29.7	32.6	9.8	31.6
DFT	3.57	4.88						
Kerisit[a]	3.66	4.82	118.1	39.7	5.8	21.5	3.5	39.2
CLAYFF[b]	3.61	4.99	50.9	19.3	13.0	32.3	8.9	15.7
Grimes[c]	3.57	4.79	117.1	35.1	0.1	11.0	−1.6	41.0
this work	3.67	4.90	118.9	39.1	5.4	23.2	2.4	39.9

[a] Reference 15. [b] Reference 10. [c] Reference 30.

The potential parameters were determined using the constraints detailed above. The charge on the hydrogen was set at 0.4*e,* and therefore, to maintain charge neutrality, this requires the hydroxide oxygen to have a charge of −1.4*e*. Schröder scaling was then applied to the system in the same way as described for the organic molecules to determine the *A* parameter in the Ca−O potential. The intermolecular O−H interaction was determined by fitting to the experimental data described above using GULP. We used a LJ 9-6 potential for this interaction. This form was chosen because previous work[29] had found it was better suited to modeling hydrogen bonding than a Buckingham potential due to the shallower gradient in the repulsive part of the potential. To test the sensitivity of the resulting parameters, constant pressure minimizations were performed on the crystal structure using a range of parameters centered on those determined during the fitting process. Intramolecular O−H interactions were described using the Morse potential determined by Baram and Parker.[25]

The resulting parameters are shown in Table 1, and the predicted structural parameters and elastic constants are shown in Table 3 where they are compared to the experimental data, DFT, and other results and calculations using other published atomistic models.[10,15,30] The fitted potentials reproduce the *c* parameter to within 0.5% of the experimental and DFT values, while the predicted *a* parameter is overestimated by 2%. Considering the other potential models for portlandite, the *c* parameter is within their error range, although both the Grimes potential and the Kerisit potential are more successful at reproducing the *a* parameter (both reproducing this to within 1% of the experimental and DFT values). However, it should be noted that both of these forcefields were fitted to the structure of portlandite, whereas our model is essentially one designed to model the polymorphs of $CaCO_3$, which has undergone relatively minor modifications, according to a set of general rules. Additionally our potential parameters successfully reproduce many of the elastic constants (particularly C_{11}, C_{12}, and C_{66}), although C_{44} is small. Of the potential parameters tested, only CLAYFF comes close to reproducing the experimental value of C_{44}, at the expense of C_{11}, C_{12}, and C_{66}, the values our models and those of Grimes and Kerisit come closest to reproducing. It is clear that our straightforward methodology can reproduce the structure of portlandite to an acceptable level

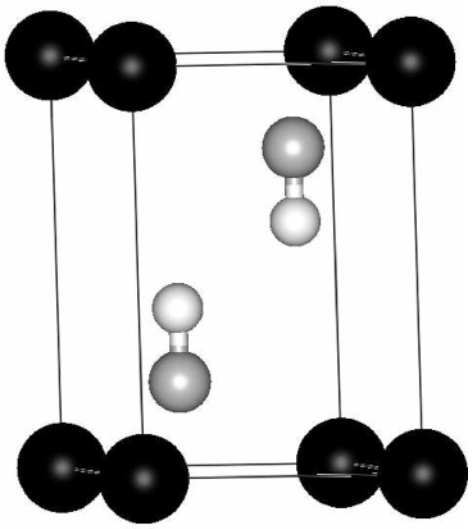

Figure 2. Crystal structure of portlandite, $Ca(OH)_2$. Key: calcium, black; oxygen, light gray; hydrogen, white.

and therefore provide us with a compatible model for Ca^{2+} interacting with a hydroxide group.

2.3.2. Calcium−Bicarbonate Interactions. In addition to considering hydroxide groups on the surface, we also required the ability to consider bicarbonated surfaces. One issue, which must be considered before fitting appropriate potential parameters, is the distribution of charge within the bicarbonate groups. For example, does the oxygen bonded to the hydrogen have a different charge to the other two bicarbonate oxygens, enabling us to use the potential model discussed in the previous section directly, or is the charge distributed equally among the three oxygens in the bicarbonate as in our model for the carbonate ion?

While it would be desirable to answer this question and validate our potential parameters using the bulk structure of calcium bicarbonate, unfortunately, $Ca(CO_3H)_2$ exists only in solution. If the solution evaporates, the following reaction occurs

$$Ca(HCO_3)_2(aq) \rightarrow CO_2(g) + H_2O(l) + CaCO_3(s) \quad (8)$$

precipitating calcite and not calcium bicarbonate.

Charge analysis could be performed on the ion in the gas phase, but it is unclear whether this would be appropriate, as the ion in our calculations will be in the solid phase and in contact with solution. To partially overcome this, we have developed a test structure based on the unit cell of $Ca(NO_3)_2$ (see Figure 3a). This structure was obtained from the EPSRC's Chemical Database Service at Daresbury Laboratory, Warrington, U.K.[31] The unit cell has a fcc structure with a space group of $PA\bar{3}$ and a cell parameter of 7.62 Å. The system was relaxed using DFT, which resulted in the cell expanding such that the cell parameter became 8.09 Å. Carbons were then substituted in place of the nitrogens, and a hydrogen was added to each carbonate group to form calcium bicarbonate (see Figure 3b) before the structure was reoptimized using DFT. During optimization, the system became monoclinic, and the relaxed cell parameters are shown in Table 2. This gives a structure that, while not observed experimentally, provides an environment for the HCO_3^- more closely related to the systems we are to study. Mülliken charge analysis was performed on the test structure, using the *CASTEP3* code, as well as Badar charge analysis using the approach of Henkelman et al.[32] to determine the distribution of charges in the bicarbonate ion. Both methods suggested that the charge was evenly distributed among the

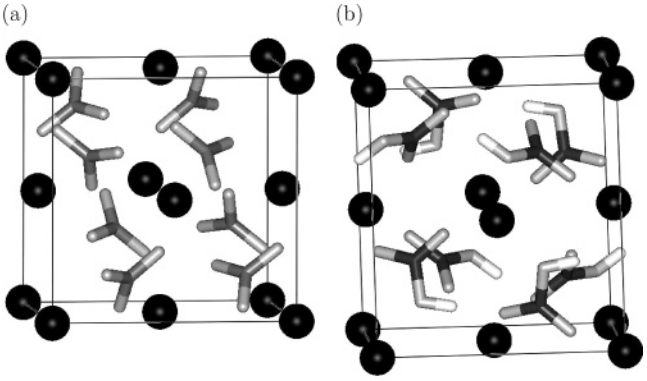

Figure 3. (a) Crystal structure of $Ca(NO_3)_2$ and (b) our presumed structure of calcium bicarbonate. Key: calcium, black; carbon; dark gray; nitrogen, medium gray; oxygen, light gray; hydrogen, white.

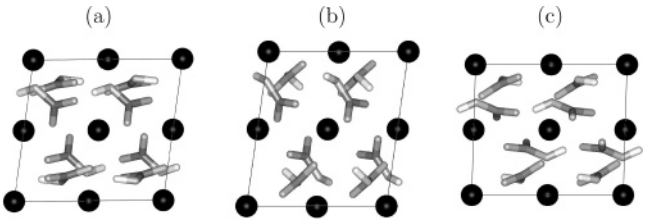

Figure 4. Relaxed calcium bicarbonate structures as viewed from the *AB* plane calculated using (a) DFT and (b and c) our potential model. Key: calcium, black; carbon, dark gray; oxygen, light gray; hydrogen, white.

bicarbonate oxygens, and thus, we have used a charge of $-0.845e$ in developing our bicarbonate model. This compares to a charge of $-1.045e$ in CO_3^{2-} and a charge of $-1.4e$ for the hydroxide oxygen.

To obtain the required potential parameters, Schröder scaling was applied to the *A* parameter of the Ca−O potential from the Pavese potential to take into account the change in charge on the oxygen atoms. The same LJ parameters used to describe the hydrogen interacting with hydroxide oxygens were used to describe the intermolecular interaction between the hydrogen and the bicarbonate oxygen. The intramolecular interaction was once again described using the O−H morse potential of Baram and Parker.[25] The resulting potential parameters are shown in Table 1.

The calculated structural parameters of calcium bicarbonate using the potential model are compared to the optimized DFT structure in Table 2. The potential parameters reproduce the DFT optimized structure to within 10%, but produce two minima. The lattice energies of the two structures are similar (−130.4 and −130.7 eV), the major difference between the two structures being the orientation of the bicarbonate groups. In the second structure, the carbonate groups are orientated, as they are in the relaxed structure from the DFT calculation (see Figure 4), with the hydrogens pointing along the *a* axis. In the first relaxed structure, the bicarbonates have rotated so the hydrogens are pointing along the *b* axis of the unit cell (Figure 4c).

Such local minima should not present a problem when we come to consider bicarbonated calcite surfaces, as the degrees of freedom available to the bicarbonate group are restricted by the surface. Additionally, since the differences in energy are relatively small, the kinetic energy present in a molecular dynamics (MD) calculation in ambient conditions should be sufficient for the bicarbonate ions to escape any local minima.

2.4. Summary. Thus far, our discussion has been based on describing a general methodology as well as discussing a new set of potential parameters. We have implemented a set of

TABLE 4: List of Number of Molecules Used in Potential Simulations and the Cell Size Used for ab Initio Simulations

molecule	number of molecules in DL_POLY cell	ab initio cell size
CH_3OH	24	1×1
H_3COCH_3	12	2×1
HCOOH	8	2×2

procedures that can be followed to generate a set of cross-term potentials for biominerals. Although we have demonstrated our methods with reference to particular forcefields, they should generally be applicable to different sets. In the next section, we test their accuracy in several different cases.

3. Potential Tests

3.1. Organic Molecules with Mineral Surfaces. The new cross-term potentials were tested by comparing the adsorption energies of small organic molecules at calcite surfaces calculated with potential-based and ab initio methods. Five-layer slabs of $CaCO_3$ terminated with the (10.4) surface were generated and optimized using the *METADISE* (Minimum Energy Techniques Applied to Dislocation Interface and Surface Energy)[33] program.

The molecules chosen for examination were methanoic acid, HCOOH, methanol, CH_3OH, and dimethylether, H_3COCH_3. The major interactions between organic molecules and mineral surfaces are expected to originate from the organic functional groups, and this selection of molecules tests three common ones, carboxylic acids, alcohols, and ethers. By using small molecules, we are better able to test our potentials against ab initio methods, but this relies on the assumption that the interactions with a large organic molecule can be broken down into independent interactions with smaller molecules. Such assumptions have been shown to give accurate results for other inorganic−organic interactions,[35,36] and given the method employed by organic forcefields (such as *AMBER*) to construct their potential sets, this seems a reasonable position.

The potentials were all generated using the methods described in the previous section. The details of all the cross-term potentials used are listed in Table 1.

The molecules were placed on a 4×3 (or 4×4 for the acid) surface of the calcite, and MD simulations, using the DL_POLY_2.16 code,[37] were performed to ensure the molecules were adsorbed at the calcite surface. Identical sets of organic molecules were adsorbed onto both surfaces. The simulations used the slab model with three-dimensional periodic boundary conditions, and a vacuum gap of ~20 Å was applied perpendicular to the surface to ensure negligible interactions between adjacent slabs. A Nosé−Hoover thermostat with a relaxation time of 0.1 ps was used to maintain a constant temperature of 10 K, and the simulation time step was 1 fs. The atoms in the middle calcite layer were fixed (to ensure the crystal structure was maintained), while the two outer layers (at each surface), along with the organic molecules, were free to move. The Ewald summation was used for all the Coulombic interactions, and a cutoff of 10.1 Å was applied to the short-range potentials. The simulations were run until the organic molecules showed no further migration (typically <0.1 ns). The number of molecules present within the cell was reduced until no significant interactions occurred between them (see Table 4 for the final numbers). The resulting geometries were then used for the comparison of the adsorption energies.

To test the potentials, a further set of MD simulations were performed using the same parameters described above with a 10 ps timelength. All the atoms, excluding the organic carbon and oxygen and those in the middle layer of the calcite slab, were free to move. The separation between the molecules and the calcite surface was systematically varied while the orientation of the molecule with respect to the calcite surface was kept constant. Adsorption energies, E_{ads}, were calculated as shown in eq 9

$$E_{ads} = \frac{(E_{system} - E_{calcite} - E_{molecule})}{N_{molecule}} \quad (9)$$

where E_{system} is the total energy of the molecules and calcite, $E_{calcite}$ is separate energy of the calcite slab, $E_{molecule}$ is the energy of the organic molecules, and $N_{molecule}$ is the number of organic molecules present within the cell.

The ab initio calculations were performed using periodic plane wave DFT as implemented in the *CASTEP3* code. The GGA and Perdew−Wang (PW91) exchange-correlation functional[38] were used. Our simulations used ultrasoft Vanderbilt pseudopotentials[39] with a cutoff of 820.0 eV. The reciprocal space integration utilized the Monkhorst−Pack sampling scheme[40] and a *k*-point spacing of 0.05 was applied. The simulation cells from DL_POLY were reduced to their smallest symmetric repeat unit (the smallest cell with a single molecule above each surface; see Table 4) to reduce the computational expense. Single-point energy calculations were performed on all the final configurations produced by the MD simulations, and adsorption energies were calculated as described in eq 9.

The comparisons of the adsorption energies calculated from the potential and ab initio methods are shown in Figure 5. The new set of potentials provide a reasonable agreement with the results of the ab initio calculations. For the ether molecule, the well depths are within 0.02 eV and the decay to zero at larger separations is very similar. Although the difference between the well depths is 0.15 eV for the acid molecule, the two curves generally match each other closely. The potentials for the alcohol molecule produce a well depth within 0.1 eV of the DFT results, but the decay of the two curves to zero shows some differences, with a more rapid decay in the potential model. The main difference between all the potential models and the ab initio method occurs at very small separations, where the DFT calculations predict a far steeper well than those seen with the potentials. Previous theoretical studies for the adsorption of methanoic acid on calcite surfaces have also used versions of the Schröder method for determining the Ca−O potentials and report adsorption energies of −0.87 eV[41] and −1.05 eV.[2] Our value, of −0.89 eV, sits between these. The differences may come from the difficulty with optimizing the position of the acid molecule on the calcite surface (which was not performed in our model) and the additional cross-term potentials we have added that are not used in either of the other models.

Although it may be possible to achieve a better match to the ab initio results by specifically refitting the potentials, we reiterate that the purpose of this exercise is to design a method that produces reliable potentials in general cases. As can clearly be seen without any major fitting work (aside from the initial fit of the O−O potential and the use of the method described by Schröder), reliable potentials can be generated for the cross-terms between the mineral and organic molecule. Also, crucially, this method should be usuable with other calcite and/or organic forcefields.

3.2. Hydrated Calcite Surfaces. So far, in our discussion on validation of the parameter sets for water on calcite surfaces, we have only considered the bulk minerals portlandite $Ca(OH)_2$, ikaite $CaCO_3 \cdot (H_2O)_6$, and our test structure of calcium bicarbonate $Ca(HCO_3)_2$. However, since the aim of this work is to consider such groups at the surfaces of calcite, we have also

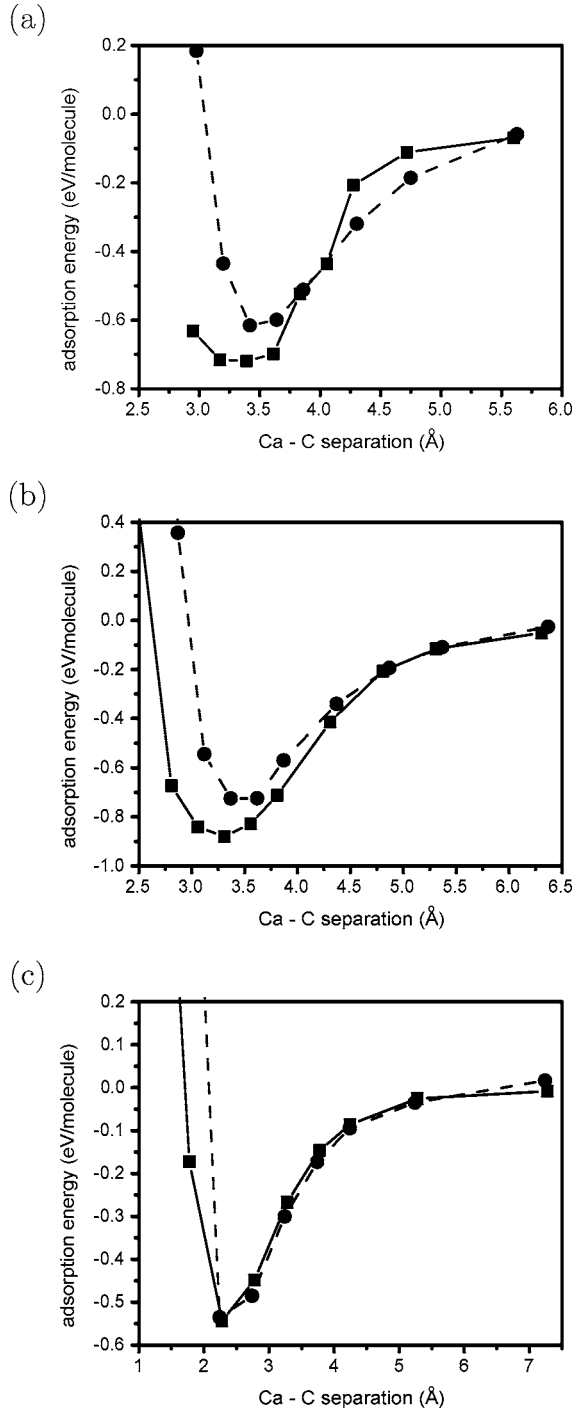

Figure 5. Comparison of adsorption energies for a (a) methanol molecule, (b) methanoic acid, and (c) dimethylether with a calcite surface calculated using the potential developed here (squares and solid line) and ab initio methods (circles and dashed line). Note that the lines are merely to guide the eye. The Ca−C separation is the distance between molecular carbon and the calcite surface.

performed a series of tests assessing their ability to reproduce the adsorption energy and hydrated/bicarbonated surface energy at the (10.4) surface of calcite. When generated using the METADISE code, the (10.4) surface cell contains six $CaCO_3$ units, and consequently, this enables us to consider a range of coverages, ranging from 16.67 to 100% coverage over a number of different adsorption sites.

Molecular water was added to the (10.4) surface of calcite by placing between zero and six water molecules 1.7 Å above the surface Ca ions, orientated such that the hydrogen atoms

TABLE 5: Calculated Hydration Energy and Surface Energy as a Function of Coverage Using the Potential Model Discussed in This Work and the Parameters Derived by Kerisit and Parker

	this work		Kerisit and Parker[a]	
	E_{hyd} (eV/H_2O)	γ (J·m^{-2})	E_{hyd} (eV/H_2O)	γ (J·m^{-2})
16.67%	−0.44	0.50	−0.21	0.54
33.33%	−0.44	0.44	−0.42	0.46
50.00%	−0.44	0.39	−0.52	0.37
66.67%	−0.44	0.33	−0.51	0.30
83.33%	−0.43	0.28	−0.40	0.31
100.00%	−0.37	0.27	−0.47	0.20

[a] Reference 29.

point away from the surface. This resulted in 64 possible configurations. All calculations were performed using the *METADISE* code. This employs a two region approach,[34] whereby atoms in the layers closest to the surface are allowed to fully relax while atoms in subsequent layers are held fixed, representing the bulk crystal. In our calculation, atoms in the first 20 Å below the surface are allowed to relax, while a further 100 Å of depth is used to represent the bulk system.

Using the energy of the relaxed structures, we define the energy of hydration in the same way as the adsorption energy in eq 9. The hydrated surface energy, γ_{hyd}, is

$$\gamma_{hyd} = \frac{(E_{wet} - (E_{bulk} + nE_{H_2O}))}{\text{Area}} \quad (10)$$

E_{H_2O} is the energy of an isolated water molecule, E_{wet} is the surface containing n water molecules, and E_{bulk} is the energy of an equivalent number of bulk $CaCO_3$ units compared to those present in the hydrated system.

The energy of hydration and the calculated hydrated surface energies are shown in Table 5 where they are compared to results obtained using the shell model potential of Kerisit and Parker.[29] Both models predict that hydrated surfaces will be more stable than the dry surface, in agreement with experimental results and DFT studies, and also indicate that there is a strong driving force for the formation of a complete monolayer of water. Comparison of the calculated surface energies shows excellent agreement between the two models, with the difference in calculated values being approximately 0.03 J·m^{-2}. The exception is the results at full coverage where the two models differ by 0.07 J·m^{-2}, although this still represents good agreement. Our potential shows little change in the hydration energy as the coverage is increased from 16.67 to 83.33% with the calculated value remaining at 0.44 eV. This is not true for the results of Kerisit and Parker, where a minimum is seen in the calculated energy at 50% coverage, although the well depth is small (∼0.1 eV) and the calculated values are close to those predicted by our model.

In addition to the adsorption tests described above, we have also performed a series of comparisons for hydration at the calcite surface with ab initio MD at a range of temperatures. A three-layer slab of calcite, terminated by the (10.4) surface, was used for the substrate. The supercell model was applied with a vacuum gap of 10.4 Å between the slabs. One water molecule was added per surface unit cell. The Vienna Ab initio Simulation Package (VASP)[42−44] was used for the ab initio MD simulations with ultrasoft pseudopotentials, a plane-wave cutoff of 297 eV, and a 1 1 1 Monkhorst-pack k-point grid. The calculations were performed using the GGA PW91 exchange-correlation functional. The time step for the MD simulations was 1 fs, and the total simulation time was 2.5 ps for each constant temperature

TABLE 6: The Mean Ca−O_{water} Separation for the Final 1.8 ps MD Simulations[d]

	separation (Å)				fraction			
temperature	VASP	CP[a]	L−B[b]	K−P[c]	VASP	CP[a]	L−B[b]	K−P[c]
300 K	2.41	2.49	2.23	2.34	1.0	0.99	1.0	1.0
600 K	2.43	2.54	2.27	2.40	1.0	0.65	1.0	0.99
900 K	2.46	2.58	2.29	2.51	1.0	0.39	0.87	0.39

[a] Current work using potential described in Table 1. [b] Lorentz Berthelot. [c] Kerisit and Parker. [d] The column labeled "fraction" gives the fraction of water molecules that are within 3 Å of the surface Ca cation. Larger separations are excluded from the calculation of the mean.

calculation (300, 600, and 900 K). The water molecule was initially placed in the lowest-energy configuration.

Atomistic MD simulations, using the DL_POLY_2.16 code, with the water/calcite potentials described earlier, were carried out for comparison with the ab intio results. A 2 × 3 surface supercell of the VASP slab was used to account for the extended range of the potentials, so the surface area in the classical simulations was 6 times larger, but identical atomic positions and coverages were maintained. The thickness of the calcite and vacuum slabs were the same. The classical simulations were also run for 2.5 ps with a time step of 1 fs. Snapshots of the configuration were captured every 0.1 ps to enable the calculation of the statistics.

To test the potentials, a comparison was made between the mean Ca−O_{water} separation in the classical and the ab initio MD simulations, for a range of temperatures. The statistics from the final 1.8 ps of the simulation were used to calculate the mean separation, and only Ca−O separations less than 3 Å were included in the calculation. The results are summarized in Table 6. Equivalent results for potentials calculated with the Kerisit and Parker potential[29] and by the standard Lorentz−Berthelot procedure, which had previously been found to overestimate the strength of the interaction between water and calcite,[2] are included in the table. The mean separation is slightly larger for the classical simulations with the current potential model than the ab initio simulations at all temperatures, but the agreement is acceptable. The Kerisit and Parker values produce smaller separations at 300 K but compare well at 600 and 900 K. The Lorentz−Berthelot results, on the other hand, give much smaller separations for all temperatures. The water molecules in the classical simulations exhibited a tendency to evaporate from the surface. The column headed "fraction" in Table 6 summarizes the average fraction of water molecules that are less than 3 Å from a surface Ca ion. It is clear that a significant number of molecules have evaporated from the surface at the elevated temperatures, even for these short simulations, and this is confirmed by visualization. In contrast, the ab initio simulations showed no evaporation up to 1500 K for 2.5 ps simulations. The 900 K simulation was extended to 3.5 ps, but the water remained on the surface, associated with the same surface Ca ion, throughout the simulation. As most biomineralization processes take place at or around 300 K, the differences exhibited at 600 and 900 K are disappointing but do not invalidate our potential set, as we achieve a good match in the temperature region we are interested in.

3.3. Bicarbonated Surfaces. Dissociated water was added to the (10.4) surface of calcite by placing an equal number (between zero and six) of OH^- groups 1.7 Å above the surface Ca ions and bicarbonating the same number of surface CO_3^{2-} groups. This resulted in 924 configurations. The same system size was used as that described for the hydrated surface when performing the energy minimization calculations.

TABLE 7: Calculated Hydroxylation Energy and Surface Energy as a Function of Coverage Using the Bicarbonate Potential Set Developed in This Work

	E_{hydrox} (eV/H_2O)	γ (J·m^{-2})
16.67%	0.172	0.585
33.33%	0.171	0.608
50.00%	0.515	0.631
66.67%	0.256	0.699
83.33%	0.452	0.864

Using the energy of the relaxed structures, we defined the energy of hydroxylation and hydroxylated surface energy in an identical way to that described previously in eqs 9 and 10. However, in both cases, the term E_{H_2O} must contain a correction to take into account the change of charge on the surface oxygens during the reaction. This is calculated using a similar approach to that described by Redfern[45,46] when studying hydroxylated oxide surfaces.

The overall reaction we are considering (in the case of hydroxylation) is the dissociation of a single water molecule on the (10.4) surface of calcite to form a bicarbonate ion and an OH^- group positioned above a surface Ca ion (eq 11).

$$Ca_nCO_{3n(104surface)} + H_2O(g) \rightarrow nCaCO_{3(n-1)}\cdot HCO_3\cdot OH_{(104surface)} \quad (11)$$

This process can be broken down into a series of steps, the energy of each of which can be calculated:

$$Ca_nCO_{3n(104surface)} \rightarrow nCa^{2+}(g) + nC^{1.135+}(g) + 3nO^{1.045-}(g) \quad (12)$$

$$Ca^{2+}(g) + C^{1.135+}(g) + 3nO^{1.045-}(g) \rightarrow CaCO_3(s) \quad (13)$$

$$CaCO_3(s) + H_2O(g) \rightarrow {}^1/_2Ca(HCO_3)_2(s) + {}^1/_2Ca(OH)_2 \quad (14)$$

$${}^1/_2Ca(HCO_3)_2(s) + {}^1/_2Ca(OH)_2 \rightarrow Ca^{2+}(g) + C^{1.135+}(g) + 3O^{0.845-}(g) + O^{1.4-}(g) + 2H^{0.4+}(g) \quad (15)$$

$$nCa^{2+}(g) + nC^{1.135+}(g) + (n-3)O^{1.045-}(g) + 3O^{0.845-}(g) + O^{1.4-}(g) + 2H^{0.4+}(g) \rightarrow nCaCO_{3(n-1)}\cdot HCO_3\cdot OH_{(104surface)} \quad (16)$$

Equation 12 represents minus the energy of the dry surface, eq 13 is the lattice energy of a single formula unit of calcite, and eq 14 is a solid-state reaction which needs to be calculated using either experimental data or ab initio calculations. Equation 15 is minus half the lattice energy of a single formula unit of calcium bicarbonate and portlandite. Finally, eq 16 is the energy of the bicarbonated surface. The sum of eqs 13−15 represents the correction factor, per water molecule, which must be included in eqs 9 and 10 and has a value of 17.43 eV/H_2O. A similar approach is followed when calculating the surface energy, except the term $Ca_nCO_{3n(104surface)}$ is replaced by an equivalent number of bulk $CaCO_3$ units.

The calculated values of the hydroxylation energy and the hydroxylated surface energy are shown in Table 7. We note that the calculated surface energies are approximately independent of coverage up to 50%, with a value of ∼0.6 J·m^{-2}. Above this value. the calculations predict that the surfaces become rapidly less stable, reflected by the surface energy increasing to 0.864 J·m^{-2}. In all cases, the calculated surface energy is

above the value for the dry surface (0.56 $J \cdot m^{-2}$), suggesting that the bicarbonate ion will not be seen on the (10.4) surface of calcite in anything other than trace amounts.

Further evidence of the unfavorable nature of the process is given by the fact that the hydroxylation energy is calculated as being positive at all coverages. The only anomaly is the calculated value of the hydroxylation energy at 50% coverage, where it is calculated as being 3 times higher than the optimum value, 33.33%, and twice the value calculated at 66.67%. At present, we are unable to provide an explanation for this. This aside, these calculations do illustrate the ability of our methodology to provide potential parameters for the modeling of bicarbonate groups on the (10.4) surface of calcium carbonate. Using the same methods described for the earlier ab initio MD simulations for hydrated calcite surfaces, we are able to calculate a value of ~1 eV/H_2O for the hydroxylation of water at the calcite surface. This value compares reasonably favorably with our values, although it is a little larger.

4. Conclusions

The requirement for reliable and transferable potentials for modeling biominerals is clear. In this paper, we have proposed a methodology for generating these potentials that does not require expensive fitting procedures and considers all of the important interactions: water−mineral, mineral−molecule, and mineral−ions. Our methodology uses existing potential sets for the various components of the system. New potentials have only been considered for the cross-term potentials that control the interactions between the different systems, e.g., the mineral−molecule interaction. Wherever possible, we have used the method described by Schröder et al.,[4] shown to work for specific biominerals (e.g., ref 5), to generate these cross-term potentials. Here, the new potentials are fitted to known mineral structures using a new set of fractional charges on the atoms that mimic the Coulombic interactions between the two biomineral systems. Whenever this approach cannot be used (e.g., for some of the water−mineral and mineral−ion interactions). we have maintained consistency by fitting new potentials to mineral structures rather than specific biomineral interactions. By the adoption of these procedures, our methodology has remained generic and can be used to generate large sets of potentials for biomineral systems.

The reliability of the methodology and the potentials it produces have been tested against ab initio and other potential sets. Good agreement can be seen between the adsorption energies for organic/water molecules and the calcite surfaces calculated using DFT and the new potential set. Also, tests for the interactions between our mineral ions and water molecules show good agreement with other previously published potential sets and ab initio results. Although the methods we describe in this paper have only been tested with regard to calcite-based systems, we anticipate that they should be applicable to other biominerals and work with a similar level of reliability.

In summary, we have demonstrated a systematic procedure for generating the essential cross-term potentials required for biomineral systems. Our methods produce reliable potentials without the need for systematic fitting and can be transferred across a range of biominerals.

Acknowledgment. The authors acknowledge funding from EPSRC under Grant Nos. GR/S80103/01 (Sheffield and University College London) and GR/S80110/01 (Cambridge). They also acknowledge computing facilities on the Mott2 machine at the Rutherford-Appleton Laboratory funded under EPSRC Grant No. GR/S84415/01. The authors would also like to thank Dr Mingjun Yang for his advice on organic molecular modeling.

References and Notes

(1) Harding, J. H.; Duffy, D. M. *J. Mater. Chem.* **2006**, *16*, 1105.
(2) Duffy, D. M.; Harding, J. H. *Langmuir* **2004**, *20*, 7630.
(3) Cormack, A. N.; Lewis, R. J.; Goldstein, A. H. *J. Phys. Chem. B* **2004**, *108*, 20408.
(4) Schröder, K.-P.; Sauer, J.; Leslie, M.; Catlow, C. R. A.; Thomas, J. M. *Chem. Phys. Lett*. **1992**, *188*, 320.
(5) de Leeuw, N. H.; Parker, S. C.; Rao, K. H. *Langmuir* **1998**, *14*, 5900.
(6) Halley, J. W.; Rustad, J. R.; Rahman, A. *J. Chem. Phys.* **1993**, *98*, 4110.
(7) Stillinger, F. H.; David, C. W. *J. Chem. Phys.* **1978**, *69*, 1473.
(8) Stillinger, F. H.; David, C. W. *J. Chem. Phys.* **1980**, *73*, 3384.
(9) Litton, D. A.; Garofalini, S. H. *J. Appl. Phys.* **2001**, *89*, 6013.
(10) Cygan, R. T.; Liang J.-J.; Kalinichev, A. G.; *J. Phys. Chem. B* **2004**, *108*, 1255.
(11) Bandura, A. V.; Kubicki, J. D. *J. Phys. Chem. B* **2003**, *107*, 11072.
(12) Berendsen, H. J. C.; Grigera, J. R.; Straatsma, T. P. *J. Phys. Chem.* **1987**, *91*, 6269.
(13) Parker, S. C.; de Leeuw, N. H.; Redfern, S. E. *Faraday Discuss.* **1999**, *114*, 381.
(14) Kerisit, S.; Cooke, D. J.; Spagnoli, D.; Parker, S. C. *J. Mater. Chem.* **2005**, *15*, 1454.
(15) Kerisit, S.; Parker, S. C.; Harding, J. H.; *J. Phys. Chem. B* **2003**, *107*, 7676.
(16) Pavese, A.; Catti, M.; Price, G. D.; Jackson, R. A. *Phys. Chem. Miner.* **1992**, *19*, 80.
(17) Pavese, A.; Catti, M.; Parker, S. C.; Wall, A. *Phys. Chem. Miner.* **1996**, *23*, 89.
(18) de Leeuw, N. H.; Parker, S. C. *J. Phys. Chem. B* **1998**, *102*, 2914.
(19) Cornell, W. D.; Cieplak, P.; Bayly, C. I.; Gould, I. R.; Merz, K. M., Jr.; Ferguson, D. M.; Spellmeyer, D. C.; Fox, T.; Caldwell, J. W.; Kollman, P. A. *J. Am. Chem. Soc.* **1995**, *117*, 5179.
(20) Jorgensen, W. L.; Chandrasekhar, J.; Madura, J. D.; Impey, R. W.; Klein, M. L. *J. Chem. Phys.* **1983**, *79*, 926.
(21) Dickens, B.; Brown, W. E. *Inorg. Chem.* **1970**, *9*, 480.
(22) de Leeuw, N. H.; Parker, S. C. *J. Chem. Soc., Faraday Trans.* **2004**, *93*, 467.
(23) Gale, J. D. *Philos. Mag. B* **1996**, *73*, 3.
(24) Gale, J. D. *J. Chem. Soc., Faraday Trans.* **1997**, *93*, 629.
(25) Baram, P. S.; Parker, S. C. *Philos. Mag. B* **1996**, *73*, 49.
(26) Desgranges, L.; Grebille, D.; Calvarin, G.; Chevrier, G.; Floquet, N.; Niepce, J. C. *Acta Crystallogr., Sect. B* **1993**, *49*, 812.
(27) Holuj, F.; Drozdowski, M.; Czajkowski, M. *Solid State Commun.* **1985**, *56*, 1019.
(28) Segall, M. D.; Lindan, P. J. D.; Probert, M. J.; Pickard, C. J.; Hasnip, P. J. J.; Clarke, S. J.; Payne, M. C. *J. Phys.:Condens. Matter* **2002**, *14*, 2717.
(29) Kerisit, S.; Parker, S. C. *J. Am. Chem. Soc.* **2004**, *126*, 10152.
(30) Chroneosa, A.; Desai, K.; Redfern, S. E.; Zacate, M. O.; Grimes, R. W. *J. Mater. Sci.* **2006**, *41*, 675.
(31) Fletcher, D. A.; McMeeking, R. F.; Parkin, D. *J. Chem. Inf. Comput. Sci*. **1996**, *36*, 746.
(32) Henkelman, G.; Arnaldsson, Jónsson, H. *Comput. Mater. Sci*. **2006**, *36*, 254.
(33) Watson, G. W.; Kelsey, E. T.; de Leeuw, N. H.; Harris, D. J.; Parker, S. C. *J. Chem. Soc., Faraday Trans.* **1996**, *92*, 433.
(34) Tasker, P. W. *AERE, Harwell Laboratory Report* **1978**, *R9130*.
(35) Sushko, M. L.; Gal, A. Yu; Shluger, A. L. *J. Phys. Chem. B* **2006**, *110*, 4853.
(36) Schravendijk, P.; Ghiringhelli, L. M.; Site, L. D.; van der Vegt, N. F. A. *J. Phys. Chem. C* **2007**, *111*, 2631.
(37) Smith, W.; Forester, T. R. *J. Mol. Graphics* **1996**, *198/199*, 796.
(38) Perdew, J. P.; Wang, Y. *Phys. Rev. B: Condens. Matter Mater. Phys.* **1992**, *45*, 13244.
(39) Vanderbilt, D. *Phys. Rev. B: Condens. Matter Mater. Phys.* **1990**, *41*, 7892.
(40) Monkhorst, H. J.; Pack, J. D. *Phys. Rev. B: Condens. Matter* **1976**, *13*, 5188.
(41) de Leeuw, N. H.; Cooper, T. G. *Cryst. Growth Des.* **2004**, *4*, 123.
(42) Kresse, G.; Hafner, J. *Phys. Rev. B: Condens. Matter Mater. Phys.* **1993**, *47*, 558.
(43) Kresse, G.; Furthmuller, J. *Phys. Rev. B: Condens. Matter Mater. Phys.* **1996**, *54*, 11169.
(44) Kresse, G.; Hafner, J. *Mater. Sci.* **1996**, *6*, 15.
(45) Redfern, S. E.; Grimes, R. W.; Rawlings, R. D. *J. Mater. Chem.* **2001**, *11*, 449.
(46) Redfern, S. E. Ph.D. Thesis, University of Bath, 1999.